Damage microstructure evolution of helium ion irradiated SiC under fusion relevant temperatures

R.W. Harrison, S. Ebert, J.A. Hinks and S.E. Donnelly

School of Computing and Engineering, University of Huddersfield, Huddersfield, HD1 3DH, UK

Abstract

In-situ transmission electron microscopy (TEM) with ion irradiation has been used to study the damage microstructure evolution of He ion irradiated 4-H SiC at nuclear fusion relevant temperatures. The SiC samples were irradiated with 20 keV He ions at 25, 400, 800 and 1200°C to a dose of 5.0 displacements per atom (DPA). At 25°C, the material fully amorphises at 1.5 DPA and no He bubble nucleation occurs up to the doses studied. At 400 and 800°C, He bubble nucleation occurs and the material remains crystalline. Bubble nucleation occurs at 2.0 DPA at 400°C but occurs at only 0.5 DPA at 1200°C. This is attributed the He atoms de-trapping from vacancies and migrating interstitially to larger He-vacancy clusters at higher temperatures, leading to faster nucleation of observable He bubbles. Helium platelets form at an irradiation temperature of 1200°C at 0.5 DPA showing a preference for nucleation between the {0001} basal planes.

Keywords: SiC, Irradiation, Fusion, Helium, In situ TEM

1 Introduction

Silicon carbide has received much attention in recent decades for potential applications in nuclear reactors due to its very high melting temperature (3000 K), good thermal and mechanical properties as well as its stability under irradiation [1], [2]. This makes it a very promising candidate for use in the extreme environments of a nuclear reactor core where the material will be exposed to extreme temperatures and radiation damage from neutron bombardment. After the Fukushima disaster, SiC-based cladding was proposed as an accident tolerant coating to replace the current zircaloy cladding [3] and is also the leading candidate for use as the protective structural layer of the TRistructural ISOtropic (TRISO) coated fuel particles for the Very High Temperature (VHTR) Generation IV nuclear reactor [4]. It is also a candidate for use as a plasma facing material (PFM) in the first wall and divertor of the DEMOnstration fusion reactor [1].

As a PFM, SiC will experience high heat fluxes and displacement damage from 14.1 MeV neutrons and charged particle bombardment. The energies of α-particles lost from the plasma as a result of D-T reactions will generally be around 100s of eV. Particles with MeV energies have also been detected escaping the plasma confinement of the Joint European Torus (JET) reactor [5]. These α particles will impact on the SiC surface resulting in variation of He implantation with depth. In addition to

impinging He atoms from the D-T reaction, He is also produced from (n,α) reactions [6]. Production of He from (n,α) reactions in SiC will vary depending on the neutron environment used with ~20 atomic parts per million (appm) of He being produced per full power year when exposed to pressurized water reactor (PWR) or fast breeder reactor (FBR) neutron spectra [6]. However, under fusion conditions such as in the DEMO reactor, ~500 appm of He will be produced per full power year from transmutation reactions (calculated using the FISPACT-II [6] neutron transport code). Thus, understanding the behaviour of He in SiC under fusion-relevant conditions (He-appm, DPA and irradiation temperature) is pertinent. There have been numerous studies into the effect of radiation damage on SiC with neutrons [7]–[11], heavy ions [9], [12] and light ions [3], [13]–[23]. However, work performed at fusion relevant temperatures (>1000°C) often consists of complex irradiation and experimental schedules, either with post-irradiation annealing or with ex-situ dual and triple ion-beam irradiations [15], [23], [24] making it difficult to determine the underlying atomistic behaviour of He. In this work we have irradiated SiC samples with He ions with in-situ transmission electron microscopy (TEM) at up to 1200°C to study He behaviour in SiC at fusion relevant temperatures.

2 Experimental

Samples were prepared for TEM from a wafer of the hexagonal close packed (HCP) polymorph, 4-H SiC (7.88° off (0001) axis in a <1120> type direction, Cree Corporation, USA) by cutting 3 mm discs using an ultrasonic disc cutter. The discs were then mechanically polished to around 100 μm thickness before dimpling with 1 μm diamond paste to a thickness of around 30 μm before Ar milling in a Precision Ion Polishing System (PIPS) to electron transparency. Samples close to the $(1\bar{1}00)$ orientation (so that the basal planes lie perpendicular to the TEM foil surface) were prepared by conventional Focused Ion Beam (FIB) lift-out technique (FEI Quanta 200 3D) and mounted on Mo grids.

In-situ ion irradiation was performed at the Microscopes and Ion Accelerators for Materials Investigations facility (MIAMI) utilising the MIAMI-1 and MIAMI-2 systems. MIAMI-1 consists of a JEOL JEM-2000FX TEM (operated at 200 kV) in which the ion beam is incident at 30° to the electron beam with an available energy range from 2–100 keV) and described elsewhere [25]. The MIAMI-2 system consists of a 350 kV ion accelerator coupled with a Hitachi–H9500 TEM (operated at 200 kV) in which the ion beam is incident at 18.7° to the electron beam. The samples were heated using either a Gatan 652 double-tilt or a Gatan 628 single-tilt heating holder. To minimise any possible synergistic effects, the electron beam was turned off during He ion irradiation. Helium bubbles were imaged using Fresnel contrast where small cavities/bubbles appear light in underfocus and dark in overfocus and cavities are assumed to be He bubbles and not voids due to their being the dominant sink for injected He atoms. MoO_3 crystals were used to calibrate the image rotation between the diffraction patterns and micrographs.

Damage and nominal He concentrations were calculated using the *Stopping Range of Ions in Matter* (SRIM-2013) Monte Carlo computer code [26]. DPA was calculated using the method proposed by Stoller et al. [27] using the 'Quick' Kinchin-Pease option of SRIM up to 5000 ions with a displacement energy of 35 eV for Si and 21 eV for C [21] with lattice and surface binding energies set to 0 eV. Helium concentrations were determined from SRIM calculations using the 'Quick' method to 99,999 ions to ensure good statistics with the foil thickness set to 50 nm. In the experimental work, samples were irradiated using 20 keV He^+ ions to achieve He–appm/DPA ratios of ~2300. The DPA rate was constant at ~2.0×10^{-3} DPA.s^{-1} for all experiments and all samples were irradiated to a dose of 5.0 DPA at temperatures of 25, 400, 800 or 1200°C.

3 Results and Discussion

3.1 Amorphisation at room temperature

Figure 1 shows bright field (BF) TEM images and selected area diffraction patterns (SAPDs) of a SiC sample irradiated at room temperature to a dose of 5.0 DPA. From the images in the sequence and the inset SADPs it can be seen that the material completely amorphises at 1.5 DPA, corresponding to a He fluence of around 3×10^{16} ions/cm^2. No bubble nucleation was observed at room temperature up to the dose studied. The amorphisation of SiC has been previously studied under neutron, ion beam and electron irradiation [12], [28], [29]. The critical dose for amorphisation in SiC at room temperature has been reported to be ~0.3 DPA for 1.5 MeV Xe ions [28], ~0.5 DPA with 0.56 MeV Si ions [12], 1.1 DPA for 70 keV He [21] and ~1.0 DPA for 2 MeV electrons [29]. The trend for the increase in DPA dose required with decreasing incident projectile mass, which has been reported previously by Snead et al. [12] is due to the decrease in residual chemical disorder per ion impact. Thus, more displacement damage is required to produce amorphisation with lighter projectiles [12]. The results of this work match well with this trend, with 20 keV He ions requiring a critical dose of 1.5 DPA to completely amorphise SiC at room temperature as compared with the lower doses for heaver ions. However, this is higher than the dose required (~1.0 DPA) in the 2 MeV electron irradiation by Inui et al. [29], and is lower than the dose required for amorphisation under fast neutron irradiation of 2.56 DPA reported by Snead et al. [12]. A possible reason for the differences in amorphisation dose in this work and that in the work of Inui et al. [29] may be that the energy of the He ions (20 keV) in this work meant that the damage peak was closer to the rear face of the TEM foil (with respect to the ion beam), resulting in the near side receiving a lower DPA than the average throughout the foil, resulting in a higher average dose to completely amorphise. The difference between the higher DPA needed for complete amorphisation in the neutron irradiation [12] case and this work may be due to the DPA rate in this work (~2.0×10^{-3} DPA.s^{-1}) being higher than the neutron case (~10^{-7} DPA.s^{-1}). Dose rate effects on the critical dose for amorpisation have previously been reported by Snead et al. [30], who found the critical dose needed for complete amorphisation increases as the flux (or DPA rate)

decreases. Liu et al. [21] irradiated SiC with 70 keV He ions and cross-sectional TEM revealed that amorphisation occurred around 1.1 DPA agreeing well with the present work.

3.2 Helium bubble characterisation at irradiation temperatures of 400°C–800°C

Figure 2 shows a sequence of BF-TEM images of SiC irradiated to 5.0 DPA at an irradiation temperature of 400°C. It can be seen from the images that, as the irradiation dose increases, there is an increase in so-called "black spot" damage accumulation which has been observed in SiC under irradiation previously and is attributed to interstitial clusters [31], [32]. These black spots, however, do not appear to grow in size and remain ~5 nm in diameter up to 5.0 DPA. Figure 3 shows a sequence of BF-TEM images of SiC irradiated to 5.0 DPA at an irradiation temperature of 800°C. Similar to the observations at 400°C, it can be seen that as the irradiation dose increases there is again an increase in black spot damage corresponding to defect cluster accumulation. However, these do not appear to grow in size as a function of dose remaining around 5–10 nm in diameter. Gao et el. [33] used molecular dynamics (MD) simulations to show the C and Si interstitials have migration activation energies of 0.77 and 1.53 eV respectively in 4H-SiC. The authors found the pre-exponential factors, D_0, for C and Si migration to be 1.69 and 3.30×10^{-3} $cm.s^{-1}$ and stated that the interstitials become thermally active at around 200 and 370°C, respectively [33]. This agrees well with the observation of no amorphisation of SiC above these temperatures in this work. Zhang et al. [34] used Rutherford backscattering spectroscopy (RBS) and nuclear reaction analysis (NRA) to study the effect of isochronal annealing on 4-H SiC samples irradiated with 1.1 MeV Al ions at room temperature. The authors [34] noted two distinct recovery stages at around 150°C and 300°C agreeing well with the predicted activation energies of C and Si interstitial mobility from ref. [33].

As the irradiation temperatures discussed in this section are much higher (400 and 800°C) than the activation energies for C and Si interstitial mobility, one might expect the growth of interstitial clusters as a function of irradiation dose via the absorption of migrating interstitial defects. Tyburska-Püschel [31] studied the effect of black spot damage on the swelling of 4-H SiC irradiation with 1 MeV Kr and 3.15 MeV C ions to 0.8 DPA at temperatures between 600–950°C. The authors assumed the clusters to be interstitial in nature; however, work by Lin et al. [35] who irradiated 3-C SiC samples with 5.1 MeV Si ions at 400°C. These clusters were predominantly found to be vacancy rich cores surrounded by interstitials atoms confirmed by high angle annular dark field (HAADF) and high resolution TEM [35]. These clusters will be immobile and thus undergo limited growth as a function of irradiation dose, with the saturation of vacancies per He ion impact in the present work (around 10 vacancies per He ion) the black spots observed in this work may be similar atomic configurations to those observed in ref. [35].

Figure 4 shows TEM images of the samples irradiated at 400 and 800°C showing He bubble nucleation and growth as a function of dose. Figure 5 shows a plot of He bubble diameter as a function of dose for both irradiation temperatures of 400 and 800°C. It can be seen from Figure 4 andFigure 5 that, in the case of the 400°C irradiation, He bubbles nucleated at 2.0 DPA but did not appear to grow significantly as a function of dose. In the case of the irradiation temperature of 400°C, it can be seen from the images in Figure 4 and the plot in Figure 6 that although the He bubble diameter did not increase observably with dose after nucleation, the areal density of the bubbles did. At the higher irradiation temperature of 800°C, He bubbles nucleated earlier at a dose of 1.0 DPA. The bubbles then grew in both size and density as can be seen from the images in Figure 4 and the plots in Figure 5 Figure 6. It can also be seen from the images in Figure 4 and the plots in Figure 5 and Figure 6 that He bubble diameter and densities were both larger at the irradiation temperature of 800°C as compared to 400°C. This is an intriguing result as the He bubbles are both larger in size and greater in areal density for the higher irradiation temperature case for the same dose and thus the same He–appm. However, this may be attributed to He atoms being trapped in monovacancies or small vacancy clusters at lower temperatures which are not visible in the TEM and at the irradiation temperature, the He atoms de-trap from these sites and migrate interstitially to larger He-vacancy clusters leading to faster nucleation and growth of He bubbles observable in the TEM.

Li et al. [36] examined the interaction between He-vacancy (He_nV_m) complexes in 6H-SiC using density functional theory (DFT) calculations to determine the binding energies of He atoms in monovacancies and small vacancy clusters. The authors found that, for He_nV_m complexes the binding energies were 0.9 eV for He_2V_1, 0.8 eV for He_2V_2, 1.3 eV for He_2V_3 and 1.7 eV for a He_2V_4 showing that an interstitial He atom would prefer to bind with a small vacancy cluster rather than a monovacancy. Sasaki et al. [8] examined the release of He from fast neutron irradiated 6H-SiC powder doped with ^{10}B to give rise to He from (n,α) transmutations noting there was an increase in He release starting from around 800°C and two further peaks were observed at ~1100 and 1260°C. Pramono et al. [37] also examined the He release rate from 6H-SiC doped with ^{10}B under a fast-neutron spectrum finding the activation energy for He diffusion to be 0.9 eV which correspond to an activation temperature of between 750–820°C (D_0 was determined to be 1.38×10^{-10} $cm^2.s^{-1}$ from [37]), agreeing well with the work by Sasaki et al. [8] and the present work, as we observe significant He bubble growth as a function of dose at irradiation temperatures of 800°C and above. This also agrees well with the work of Jung [38] who measured He release from SiC samples annealed to 827°C. Jung [38] found an activation energy for He interstitial diffusion of 1.14 eV and D_0 was determined to be 1.1×10^{-6} $cm^2.s^{-1}$.

The activation energy for self-diffusion (which is attributed to vacancy migration) of Si has been reported to be 7–8 eV in 6H-SiC [39] and 9.5 eV in 3C-SiC [40] and for C has been reported to be

5.8–7.8 eV in 3C-SiC [41] and 7.4–8.2 eV in 6H-SiC [42]. At a temperature of 400°C Lin et al. [35] reported the both Si and C vacancies to be immobile with diffusion rates of 4×10^{-15} $cm^2.s^{-1}$and 9×10^{-9} $cm^2.s^{-1}$, respectively. Thus, it is clear that both vacancy migration processes occur well above the temperatures reported in this section and previous works [8], [37]. Similarly, the lowest temperature for the observation of void nucleation in neutron irradiated SiC has been reported to be 1250°C [43]. This rules out a He_1V_1 complex (and any other larger He_nV_m) as the diffusing defect that gives rise to larger diameter and higher areal density of He bubbles observed in this work at irradiation temperatures of 800°C and above. From the attractive binding energies for He_nV_m complexes calculated by Li et al. [36] and the fact that the 20 keV He ions used in this work will create 10 vacancies per ion (according to SRIM calculations), it can be assumed that an injected He atom will trap in a monovacancy or small vacancy cluster rather than interstitially in 4H-SiC. A mechanism whereby He is trapped in a monovacancy or small vacancy cluster and the He diffusion increases at temperatures much below the Si or C vacancy migration energy must require the trapped He atom to go back into solution. Pramono et al. [37] attributed the higher release rate of He at ~800°C with an activation energy of ~0.9 eV to a dissociative and interstitial diffusion mechanism, whereby the He atoms de-trap from irradiation induced defects and subsequently undergo interstitial diffusion. As previously discussed, Li et al. [36] found that the binding energy of He in He_nV_m complexes increases as the number of vacancies increases so that He atoms will preferentially bind to a larger He_nV_m rather than a monovacancy.

At higher temperatures, a He atom is more likely to de-trap from a monovacancy and retrap in a small He-vacancy cluster (with a stronger binding energy). This could give rise to the observation in this work that He bubble nucleation occurs at a lower DPA at the irradiation temperature of 800°C. The higher irradiation temperature of 800°C leads to the trapping of a larger number of He atoms at vacancy clusters potentially leading to the growth of larger He_nV_m clusters of observable size in the microscope. However, if vacancy migration mechanisms are not active then the arriving He atoms will begin to over-pressurize the He_nV_m cluster. Li et al. [36] calculated that a cluster of 7 vacancies could accommodate 14 He atoms before the addition of another He atom became endothermic. Without further vacancies arriving via thermal migration, the cluster may grow by one of two possible mechanisms: i) trap-mutation, whereby over pressurization leads to emission of a self-interstitial atom (SIA) from the cluster creating an additional vacancy; or ii) irradiation enhanced defect production and diffusion, whereby a cascade may impinge close to a pre-existing He_nV_m cluster and supply vacancies. This combination of He de-trapping from monovacancies and interstitial migration to a larger He_nV_m clusters associated with an activation energy of 0.9 eV [37] (activation temperature of ~750–820°C) could then lead to the observations in our work of: i) the nucleation of observable He bubbles at lower DPA at the irradiation temperature of 800°C compared to irradiation at 400°C; ii) an

increase in He bubble diameter with increasing dose at higher irradiation temperatures; and iii) a greater areal density of observable He bubbles at higher irradiation temperatures.

3.2 Helium platelet characterisation at an irradiation temperature of 1200°C

Figure 7 shows a sequence of BF-TEM images of SiC irradiated to 5.0 DPA at an irradiation temperature of 1200°C. Helium platelets with associated strain fields are formed and these increase in diameter as the irradiation dose increases. Helium platelets are 2D structures and are anticipated to form when the vacancy supply for formation of 3D defects (i.e. cavities) is limited [44], [45]. Helium platelets have been reported in 4H and 6H-SiC [3], [13], [14], [16]–[19], [46] and have also been observed in He ion-irradiated metals [47]–[49]. At the irradiation temperature of 1200°C, He diffusion via the trap dissociation (monovacancy de-trapping) and interstitial migration mechanisms will be very fast and will lead to the rapid arrival of He at He_nV_m clusters leading to very high pressures. As Si and C vacancy migration will still be low at this temperature (activation energies between 5–9 eV [39]–[42]), platelet growth occurs via trap mutation and ejection of SIAs from the platelet edge forming an interstitial dislocation loop which remains associated with the platelet [50].

Figure 8a–c shows TEM images of He platelet evolution as a function of dose and Figure 8d shows the SADP of the area in the images. It can be seen from Figure 8a that at 1.0 DPA the cavity is a continuous feature indicating that the platelet is a single, over-pressurized He filled cavity as it gives rise to observable diffraction contrast from its strain field. However, as the dose and the diameter of the platelet increase, fine structure is visible and individual bubbles can be discerned. This indicates that the evolution of the He platelets into He bubble discs has occurred. The size of the platelets and bubble discs increases from ~45 nm in diameter at 1.0 DPA to around 90 nm at 2.0 DPA (shown in Figure 8b) and around 105 nm at 5.0 DPA (shown in Figure 8c). This collapse corresponds to a critical diameter of the He platelets of ~45 nm (at 1.0 DPA) with a concentration of ~2300 He-appm in the sample.

Chen et al. [17] examined the effect of annealing 26.3 MeV He ion irradiated 4H-SiC up to 1727°C. The authors noted that platelets formed after annealing to temperatures up to ~1050°C with 600 He–appm. At annealing temperatures of ~1050–1450°C, Chen et al. [17] found that the platelets became bubble discs through collapse into individual bubbles. Chen et al. [17] observed a maximum diameter of the He platelets before collapse into bubble discs of around 35 nm for 4H-SiC samples implanted to 2450 He–appm, agreeing well with the critical diameter of 45 nm found in this work. Although it might be expected that a single bubble would be the more energetically favourable structure than a disc of small bubbles, Finnis et al. [51] found that a cluster of smaller bubbles has a lower total energy than a single larger bubble due to elastic interaction between the bubbles. The reason for the initial formation of He platelets is thus unclear – although this takes place under conditions where equilibrium conditions may not be established. No quantitative theory of platelet formation has yet

been developed. However, it has been proposed that the kinetics of He absorption at the edge of the platelet and the trap mutation process make the platelet the kinetically more favourable defect [51].

Helium platelets have been observed to form in other materials, nucleating between {110} planes in Mo [49], {111} in Ni [48] and {0001} in Ti [47] and SiC [14], [20], [46]. This represents a tendency for the platelets to nucleate between the close-packed planes which have the largest distance between them. D'Olieslaeger et al. [48] simulated growth of 2-D planar He platelets in Ni, showing that the platelets grow by emission of SIAs in the direction of the close-packed plane, which is associated with the lower energy activation for trap mutation. Chen et al. [17] found that in bulk irradiated samples He platelets and bubble discs in 4H and 6H-SiC predominantly formed on the basal (0001) plane. However, a few percent formed on the prismatic-I $(01\bar{1}0)$ planes and prismatic-II $(2\bar{1}\bar{1}0)$ planes [17]. Shen et al. [3] observed the formation of He bubble discs using 3.5 keV He ions at temperatures between 700–900°C using in-situ TEM. This is contrary to our findings for irradiations at 800°C where no platelets or bubble discs were observed at any dose at an irradiation temperature of 800°C. However, this is likely due to the much lower concentration of He implanted in our work, resulting in lower agglomeration of He atoms and thus much slower kinetics of He absorption at vacancy clusters or arrival of He to agglomerations between close-packed planes.

Shen et al. [3] also noted that the bubble discs lay on prismatic-I $\{10\bar{1}0\}$ planes and no platelets were observed on the basal plane. Figure 9a shows a SiC sample orientated close to the [0001] direction (as shown by the corresponding SADP in Figure 9b) irradiated with 20 keV He ions to 2.0 DPA at 1200°C. From figure 9a it can be seen that there is a dominance (~70%) of He bubble discs nucleated face-on (i.e. where the platelets lie parallel with the surface) between {0001} planes with some forming on the prismatic-I $\{01\bar{1}0\}$ type planes. Hueging et al. [52] examined He platelet nucleation in (001)-orientated Si irradiated with 40 keV He ions to a implantation depth of ~400 nm and observed a dominance of platelet formation parallel with the (001) surface. The authors [52] attributed this to the free surface reducing the stress field caused by platelets orientated parallel to the surface as its stress field is more pronounced above and below the platelet. Frabboni et al. [53] examined the annealing of Si samples implanted with He using in-situ TEM and noted the formation of He platelets at ~300°C. The irradiations [53] were performed on samples of (001) orientation and plan-view TEM samples showed predominantly face-on (001) and some (010) edge-on platelets (i.e. where the platelets lie perpendicular to the surface) agreeing with Hueging et al. [52] with surface effects dominating the favourable nucleation orientation. Figure 10a shows a SiC sample orientated close to the $[1\bar{1}00]$ direction (so that the {0001} planes are perpendicular to the surface) irradiated to 2.0 DPA at 1200°C. Figure 10b shows the SADP of the area in Figure 10a showing that the predominant platelet orientation is parallel to the {0001} planes. The platelets preferentially form edge-on in the TEM foil – with ~70% forming between the {0001} planes and ~30% face-on. This has shown that even when

the basal planes are perpendicular to the surface, the relaxation induced due to the proximity of the two surfaces in the TEM foil has little impact with the basal plane remaining the energetically more-favourable nucleation plane.

This is of great importance for plasma-facing components as He ion bombardment from the plasma will generally have subthreshold displacement energies and so is optimal for platelet formation (i.e. He concentration >> vacancy concentration). This may be of consequence for all potential HCP materials under consideration for use in first wall and divertor components such as titanium alloys [54] and MAX phases (where M = early transition metal, A = group A element and X = carbon or nitrogen) [4]. Figure 11 shows a plot of critical threshold dose for both DPA and He fluence for bubble nucleation as a function of irradiation temperature showing a linear relationship. The error bars extending in the negative direction in the plots of critical DPA and dose are due to the electron beam being off during irradiation and so bubble nucleation may have occurred at any point during that irradiation step. This indicates that at a He-appm/DPA ratio of ~2300 and at an irradiation temperature of 1200°C (which is the anticipated operating temperature of the plasma facing side of the PFM) He platelet and bubble nucleation will occur at around 0.5 DPA (~1150 He–appm).

4 Conclusions

Samples of 4H-SiC have been irradiated with 20 keV He ions and observed using in-situ TEM giving a He-appm/DPA ratio of ~2300 at 25, 400, 800 and 1200°C up to a total dose of 5.0 DPA to mimic conditions anticipated under fusion reactor conditions. The main conclusions from this work are:

i) At an irradiation temperature of 25°C, SiC amorphises at 1.5 DPA attributed to a lack of interstitial mobility at this temperature.

ii) Helium bubbles nucleate at lower DPA as the irradiation temperature is increased concomitantly with an increase in He bubble size and areal density. Nucleation dose decreases from 2.0 DPA at an irradiation temperature of 400°C to 0.5 DPA at 1200°C.

iii) The increase in He bubble diameter and areal density with irradiation temperature is attributed to smaller bubbles and He_nV_m complexes not being visible in the TEM at lower irradiation temperatures due to a trap dissociation and interstitial diffusion. The He atoms de-trap from monovacancies and subsequently interstitially diffuse and retrap at He-vacancy clusters which then grow via SIA ejection and trap mutation.

iv) Helium platelets formed at an irradiation temperature of 1200°C and predominantly nucleate between the {0001} basal planes regardless of surface relaxation effects. Helium bubble platelets were observed to collapse into bubble discs at 2.0 DPA corresponding to a fluence of ~5×10^{16} ions/cm^2.

Acknowledgments

The authors are grateful to the EPSRC for financial support of this project through grants EP/M011135/1, EP/E017266/1 and EP/M028283/1.

References

[1] A. Iveković, S. Novak, G. Dražić, D. Blagoeva, and S. G. de Vicente, "Current status and prospects of SiCf/SiC for fusion structural applications," *J. Eur. Ceram. Soc.*, vol. 33, no. 10, pp. 1577–1589, 2013.

[2] Y. Katoh, L. L. Snead, I. Szlufarska, and W. J. Weber, "Radiation effects in SiC for nuclear structural applications," *Curr. Opin. Solid State Mater. Sci.*, vol. 16, no. 3, pp. 143–152, 2012.

[3] Q. Shen, G. Ran, J. Hinks, S. E. Donnelly, L. Wang, and N. Li, "In situ observation of microstructure evolution in 4H-SiC under 3.5 keV He+ irradiation," *J. Nucl. Mater.*, vol. 471, pp. 149–153, 2016.

[4] W. E. Lee, E. Giorgi, R. Harrison, A. Maître, and O. Rapaud, "Nuclear Applications for Ultra-High Temperature Ceramics and MAX Phases," in *Ultra-High Temperature Ceramics*, John Wiley & Sons, Inc, 2014, pp. 391–415.

[5] D. S. Darrow, F. E. Cecil, V. Kiptily, K. Fullard, A. Horton, and A. Murari, "Observation of alpha particle loss from JET plasmas during ion cyclotron resonance frequency heating using a thin foil Faraday cup detector array," *Rev. Sci. Instrum.*, vol. 81, no. 10, p. 10D330, Oct. 2010.

[6] J.-C. Sublet, J. W. Eastwood, and J. G. Morgan, "EASY-II Renaissance: n, p, d, α, γ-induced Inventory Code System," *Nucl. Data Sheets*, vol. 118, pp. 115–117, 2014.

[7] X. Chen, W. Zhou, Q. Feng, J. Zheng, X. Liu, B. Tang, J. Li, J. Xue, and S. Peng, "Irradiation effects in 6H-SiC induced by neutron and heavy ions: Raman spectroscopy and high-resolution XRD analysis," *J. Nucl. Mater.*, vol. 478, pp. 215–221, 2016.

[8] K. Sasaki, T. Yano, T. Maruyama, and T. Iseki, "Helium release and microstructure of neutron-irradiated SiC ceramics," *J. Nucl. Mater.*, vol. 179–181, no. PART 1, pp. 407–410, 1991.

[9] H. Zang, W. Jiang, W. Liu, A. Devaraj, D. J. Edwards, C. H. Henager, R. J. Kurtz, T. Li, C. He, D. Yun, and Z. Wang, "Vacancy effects on the formation of He and Kr cavities in 3C-SiC irradiated and annealed at elevated temperatures," *Nucl. Instruments Methods Phys. Res. Sect. B Beam Interact. with Mater. Atoms*, vol. 389–390, pp. 40–47, 2016.

[10] T. Yano, H.Miyazaki, M.Akiyoshi, and T.Iseki, "X-ray diffractometry and high-resolution electron microscopy of neutron-irradiated SiC to a fluence of 1 . 9 = 10 27 n r m 2," *J. Nucl. Mater.*, vol. 253, pp. 78–86, 1998.

[11] L. L. Snead, Y. Katoh, T. Koyanagi, K. Terrani, and E. D. Specht, "Dimensional isotropy of 6H and 3C SiC under neutron irradiation," *J. Nucl. Mater.*, vol. 471, pp. 92–96, 2016.

[12] L. . Snead, S. J. Zinkle, J. . Hay, and M. . Osborne, "Amorphization of SiC under ion and neutron irradiation," *Nucl. Instruments Methods Phys. Res. Sect. B Beam Interact. with Mater. Atoms*, vol. 141, no. 1–4, pp. 123–132, 1998.

[13] J. F. Barbot, S. Leclerc, M. L. David, E. Oliviero, R. Montsouka, F. Pailloux, D. Eyidi, M. F. Denanot, M. F. Beaufort, A. Declémy, V. Audurier, and C. Tromas, "Helium implantation into 4H-SiC," *Phys. Status Solidi Appl. Mater. Sci.*, vol. 206, no. 8, pp. 1916–1923, 2009.

[14] J. Chen, P. Jung, and H. Trinkaus, "Evolution of Helium Platelets and Associated Dislocation Loops in α-SiC," *Phys. Rev. Lett.*, vol. 82, no. 13, pp. 2709–2712, 1999.

[15] A. Hasegawa, S. Miwa, S. Nogami, A. Taniguchi, T. Taguchi, and K. Abe, "Study of hydrogen effects on microstructural development of SiC base materials under simultaneous irradiation with He- and Si-ion irradiation conditions," *J. Nucl. Mater.*, vol. 329–333, no. 1–3 PART A, pp. 582–586, 2004.

[16] Q. Shen, W. Zhou, G. Ran, R. Li, Q. Feng, and N. Li, "Evolution of helium bubbles and discs in irradiated 6H-SiC during post-implantation annealing," *Materials (Basel).*, vol. 10, no. 2, 2017.

[17] J. Chen, P. Jung, and H. Trinkaus, "Microstructural evolution of helium-implanted α-SiC," *Phys. Rev. B - Condens. Matter Mater. Phys.*, vol. 61, no. 19, pp. 12923–12932, 2000.

[18] C. H. Chen, Y. Zhang, Y. Wang, M. L. Crespillo, C. L. Fontana, J. T. Graham, G. Duscher, S. C. Shannon, and W. J. Weber, "Dose dependence of helium bubble formation in nano-engineered SiC at 700°C," *J. Nucl. Mater.*, vol. 472, pp. 153–160, 2016.

[19] C. H. Chen, Y. Zhang, E. Fu, Y. Wang, M. L. Crespillo, C. Liu, S. Shannon, and W. J. Weber, "Irradiation-induced microstructural change in helium-implanted single crystal and nano-engineered SiC," *J. Nucl. Mater.*, vol. 453, no. 1–3, pp. 280–286, 2014.

[20] K. Hojou and K. Izui, "Bubbles in SiC crystals formed by helium ion irradiation at high temperatures," *J. Nucl. Mater.*, vol. 160, no. 2–3, pp. 147–152, 1988.

[21] M. Liu, X. Yang, Y. Gao, R. Liu, H. Huang, X. Zhou, and T. K. Sham, "Investigation of the damage behavior in CVD SiC irradiated with 70 keV He ions by NEXAFS, Raman and TEM," *J. Eur. Ceram. Soc.*, vol. 37, no. 4, pp. 1253–1259, 2017.

[22] K. Hojou, S. Furuno, K. N. Kushita, H. Otsu, Y. Furuya, and K. Izui, "In situ EELS and TEM observation of silicon carbide irradiated with helium ions at low temperature and successively annealed," *Nucl. Instruments Methods Phys. Res. Sect. B-Beam Interact. with Mater. Atoms*, vol. 116, no. 1–4, pp. 382–388, 1996.

[23] A. Deslandes, M. C. Guenette, L. Thomsen, M. Ionescu, I. Karatchevtseva, and G. R. Lumpkin, "Retention and damage in 3C-SiC irradiated with He and H ions," *J. Nucl. Mater.*, vol. 469, pp. 187–193, 2016.

[24] T. Taguchi, N. Igawa, S. Miwa, E. Wakai, S. Jitsukawa, L. L. Snead, and A. Hasegawa, "Synergistic effects of implanted helium and hydrogen and the effect of irradiation temperature on the microstructure of SiC/SiC composites," *J. Nucl. Mater.*, vol. 335, no. 3, pp. 508–514, 2004.

[25] J. A. Hinks, J. A. van den Berg, and S. E. Donnelly, "MIAMI: Microscope and ion accelerator for materials investigations," *J. Vac. Sci. Technol. A Vacuum, Surfaces, Film.*, vol. 29, no. 2, p. 21003, 2011.

[26] J. F. Ziegler, "Stopping of energetic light ions in elemental matter," *J. Appled Phys.*, vol. 85, no. 3, p. 1249, 1999.

[27] R. E. Stoller, M. B. Toloczko, G. S. Was, A. G. Certain, S. Dwaraknath, and F. A. Garner, "On the use of SRIM for computing radiation damage exposure," *Nucl. Instruments Methods Phys. Res. Sect. B Beam Interact. with Mater. Atoms*, vol. 310, pp. 75–80, 2013.

[28] W. J. Weber, L. M. Wang, and N. Yu, "The irradiation-induced crystalline-to-amorphous phase transition in α-SiC," *Nucl. Instruments Methods Phys. Res. B*, vol. 116, no. 1–4, pp. 322–326, 1996.

[29] H. Inui, H. Mow, and H. Fujita, "Electron irradiation induced crystalline-amorphous transition in ceramics," *Acta Metall.*, vol. 37, no. 5, pp. 1337–1342, May 1989.

[30] L. L. Snead, S. J. Zinkle, W. S. Eatherly, D. K. Hensley, N. L. Vaughn, and J. W. Jones, "Dose Rate Dependence of the Amorphization of Silicon Carbide," *MRS Proc.*, vol. 540, 1998.

[31] B. Tyburska-Püschel, Y. Zhai, L. He, C. Liu, A. Boulle, P. M. Voyles, I. Szlufarska, and K. Sridharan, "Size distribution of black spot defects and their contribution to swelling in irradiated SiC," *J. Nucl. Mater.*, vol. 476, pp. 132–139, 2016.

[32] C. Liu, L. He, Y. Zhai, B. Tyburska-Püschel, P. M. Voyles, K. Sridharan, D. Morgan, and I. Szlufarska, "Evolution of small defect clusters in ion-irradiated 3C-SiC: Combined cluster dynamics modeling and experimental study," *Acta Mater.*, vol. 125, pp. 377–389, 2017.

[33] F. Gao, W. J. Weber, M. Posselt, and V. Belko, "Atomic Computer Simulations of Defect Migration in 3C and 4H-SiC," *Mater. Sci. Forum*, vol. 457–460, pp. 457–460, 2004.

[34] Y. Zhang, W. J. Weber, W. Jiang, A. Hallén, and G. Possnert, "Damage evolution and recovery on both Si and C sublattices in Al-implanted 4H-SiC studied by Rutherford backscattering spectroscopy and nuclear reaction analysis," *J. Appl. Phys.*, vol. 91, no. 10 I, pp. 6388–6395, 2002.

[35] Y. R. Lin, L. G. Chen, C. Y. Hsieh, M. T. Chang, K. Y. Fung, A. Hu, S. C. Lo, F. R. Chen, and J. J. Kai, "Atomic Configuration of Point Defect Clusters in Ion-Irradiated Silicon Carbide," *Sci. Rep.*, vol. 7, no. 1, pp. 1–6, 2017.

[36] R. Li, W. Li, C. Zhang, P. Zhang, H. Fan, D. Liu, L. Vitos, and J. Zhao, "He-vacancy interaction and multiple He trapping in small void of silicon carbide," *J. Nucl. Mater.*, vol. 457, pp. 36–41, 2015.

[37] Y. Pramono, K. Sasaki, and T. Yano, "Release and Diffusion Rate of Helium in Neutron-Irradiated SiC," *J. Nucl. Sci. Technol.*, vol. 41, no. 7, pp. 751–755, 2004.

[38] P. Jung, "Diffusion and retention of helium in graphite and silicon carbide," *J. Nucl. Mater.*, vol. 191–194, pp. 377–381, 1992.

[39] J. D. Hong, R. F. Davis, and D. E. Newbury, "Self-diffusion of silicon-30 in alpha-SiC single crystals," *J. Mater. Sci.*, vol. 16, no. 9, pp. 2485–2494, 1981.

[40] M. H. Hon, R. F. Davis, and D. E. Newbury, "Self-diffusion of 30Si in polycrystalline β-SiC," *J. Mater. Sci.*, vol. 15, no. 8, pp. 2073–2080, 1980.

[41] M. H. Hon and R. F. Davis, "Self-diffusion of 14C in polycrystalline beta-SiC," *J. Mater. Sci.*, vol. 14, no. 10, pp. 2411–2421, 1979.

[42] J. D. Hong and R. F. Davis, "Self-Diffusion of Carbon-14 in High-Purity and N-Doped α-SiC Single Crystals," *J. Am. Ceram. Soc.*, vol. 63, no. 9–10, pp. 546–552, Sep. 1980.

[43] L. L. Snead, T. Nozawa, Y. Katoh, T.-S. Byun, S. Kondo, and D. A. Petti, "Handbook of SiC properties for fuel performance modeling," *J. Nucl. Mater.*, vol. 371, no. 1, pp. 329–377, 2007.

[44] O. El-Atwani, J. A. Hinks, G. Greaves, S. Gonderman, T. Qiu, M. Efe, and J. P. Allain, "In-situ TEM observation of the response of ultrafine- and nanocrystalline-grained tungsten to extreme irradiation environments," *Sci. Rep.*, vol. 4, no. 1, p. 4716, 2015.

[45] O. El-Atwani, K. Hattar, J. A. Hinks, G. Greaves, S. S. Harilal, and A. Hassanein, "Helium bubble formation in ultrafine and nanocrystalline tungsten under different extreme conditions," *J. Nucl. Mater.*, vol. 458, pp. 216–223, Mar. 2015.

[46] C. H. Zhang, S. E. Donnelly, V. M. Vishnyakov, J. H. Evans, T. Shibayama, and Y. M. Sun, "A study of the formation of nanometer-scale cavities in helium-implanted 4H-SiC," *Nucl. Instruments Methods Phys. Res. Sect. B Beam Interact. with Mater. Atoms*, vol. 218, no. 1–4, pp. 53–60, 2004.

[47] T. Schober and H. Trinkaus, "3He bubble formation in titanium tritides at elevated temperatures A TEM study," *Philos. Mag. A*, vol. 65, no. 5, pp. 1235–1247, 1992.

[48] M. D'Olieslaeger, L. De Schepper, G. Knuyt, and L. M. Stals, "Planar helium bubble arrays in nickel," *J. Nucl. Mater.*, vol. 138, no. 1, pp. 27–30, 1986.

[49] J. H. Evans, A. van Veen, and L. M. Caspers, "Formation of helium platelets in molybdenum," *Nature*, vol. 291, no. 5813, pp. 310–312, May 1981.

[50] M. D'Olieslaeger, G. Knuyt, L. De Schepper, and L. M. Stals, "Atomistic computer simulation of the growth of helium platelets in nickel," *Philos. Mag. Part B*, vol. 63, no. 6, pp. 1335–1341, 1991.

[51] M. W. Finnis, A. Van Veen, and L. M. Caspers, "The energy of helium filled platelets and bubbles in molybdenum," *Radiat. Eff.*, vol. 78, no. 1–4, pp. 121–132, 1983.

[52] N. Hueging, M. Luysberg, H. Trinkaus, K. Tillmann, and K. Urban, "Quantitative pressure and strain field analysis of helium precipitates in silicon," *J. Mater. Sci.*, vol. 41, no. 14, pp. 4454–4465, 2006.

[53] S. Frabboni, F. Corni, C. Nobili, R. Tonini, and G. Ottaviani, "Nanovoid formation in helium-implanted single-crystal silicon studied by in situ techniques," *Phys. Rev. B*, vol. 69, no. 16, p. 165209, Apr. 2004.

[54] M. Victoria, N. Baluc, and P. Spätig, "Structural materials for fusion reactors," *Nucl. Fusion*, vol. 41, no. 8, pp. 1047–1053, 2002.

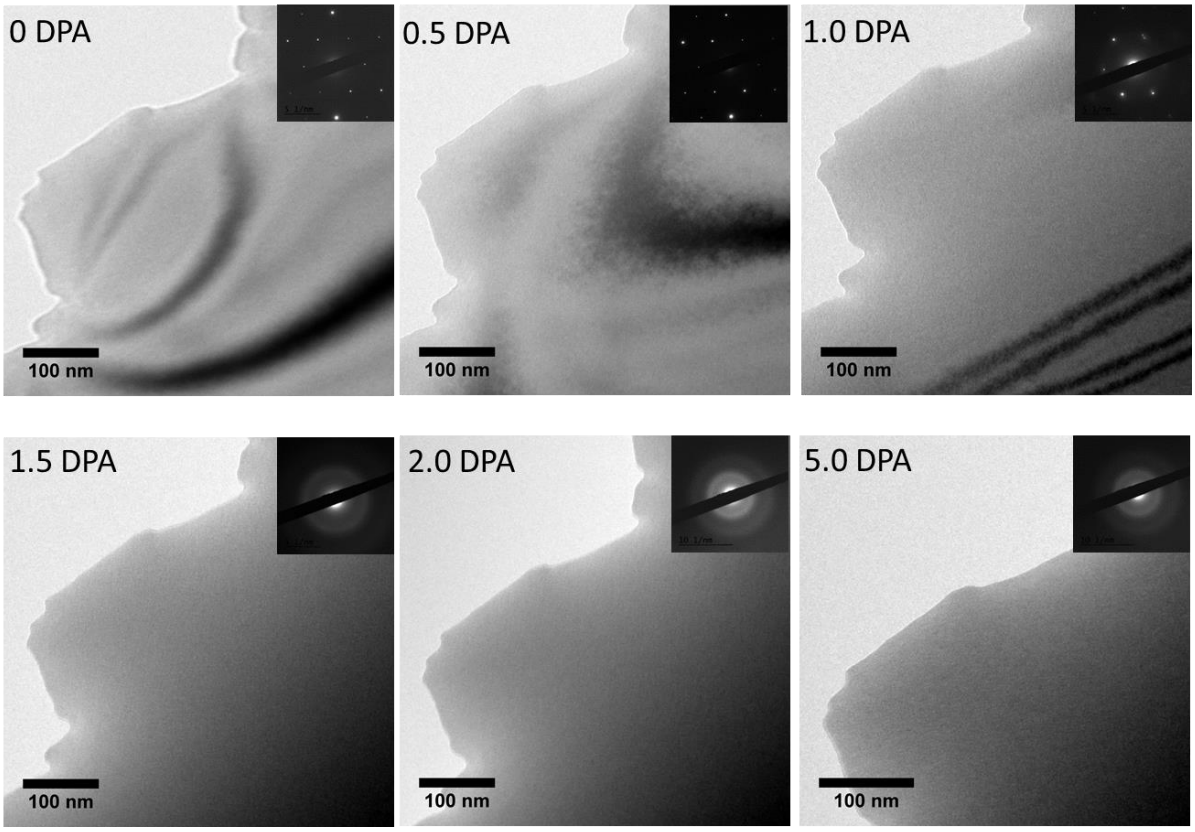

Figure 1. BF-TEM images of SiC irradiated with 20 keV He ions at room temperature showing the same area, labelled with damage dose received (DPA) and SADPs inset showing that the material becomes fully amorphous at 1.5 DPA.

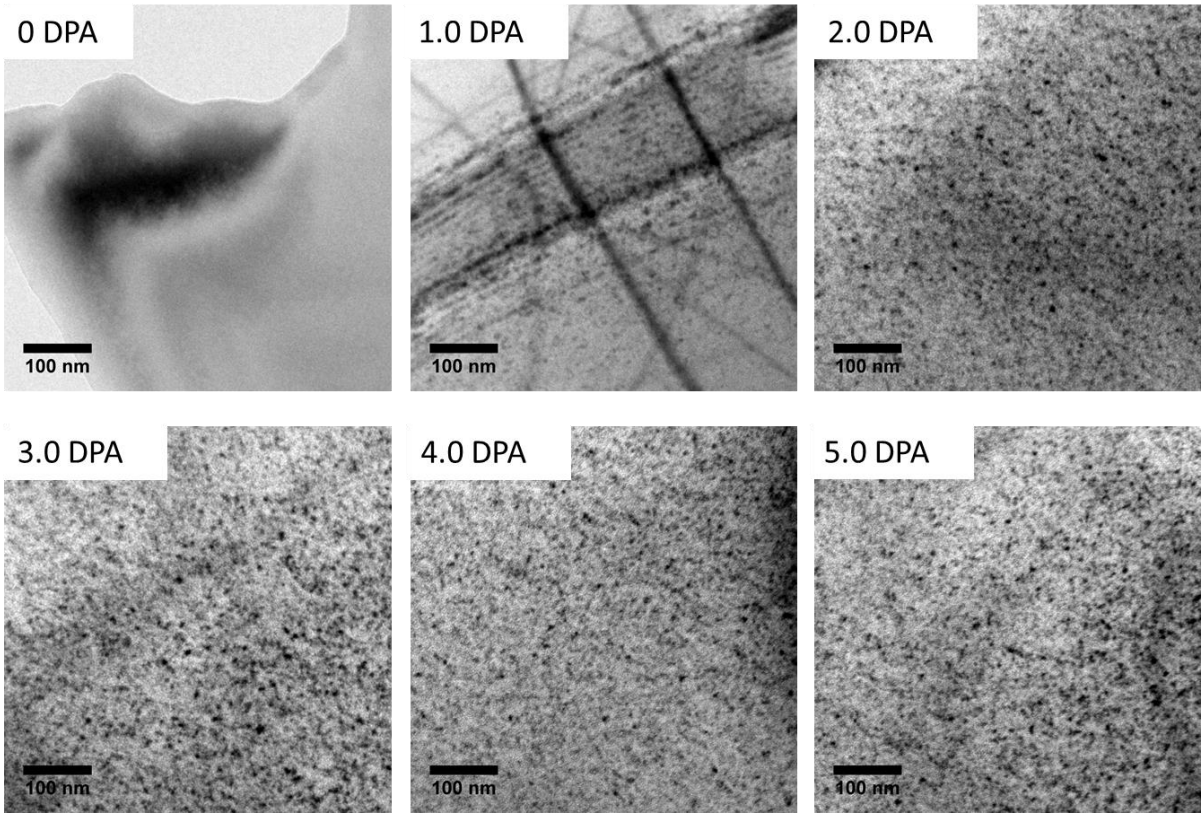

Figure 2. BF-TEM images of SiC irradiated with 20 keV He ions at 400°C (1.5µm of underfocus) labelled with damage dose received (DPA) showing the nucleation and growth of defect clusters and He bubbles (higher magnification images of He bubbles in figure 4).

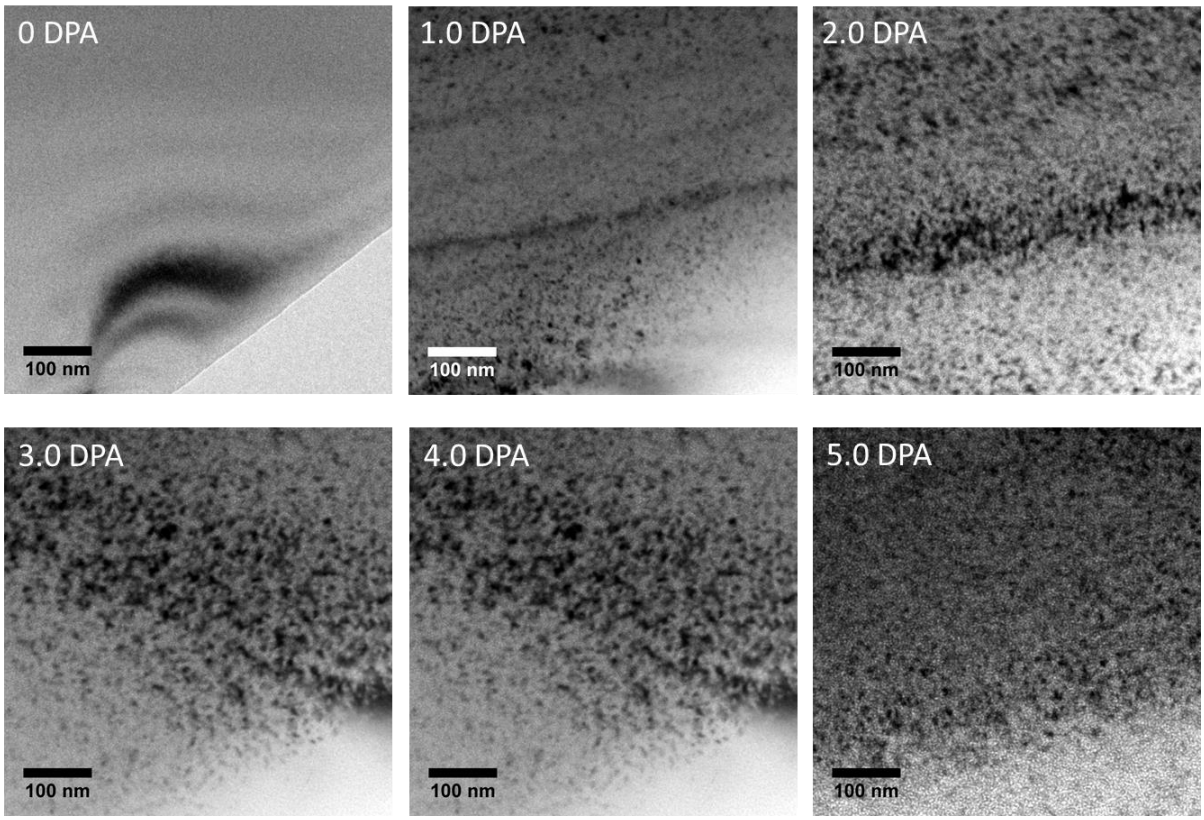

Figure 3. BF-TEM images of SiC irradiated with 20 keV He ions at 800°C (1.5 µm of underfocus) labelled with damage dose received (DPA) showing the nucleation and growth of defect clusters and He bubbles.

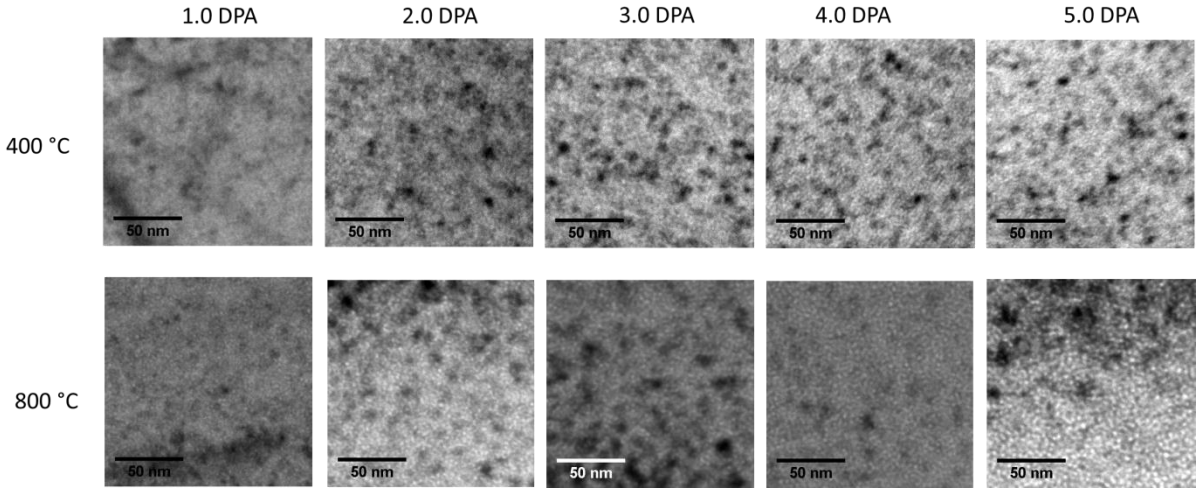

Figure 4. BF-TEM images of SiC irradiated with 20 keV He ions at 400 and 800°C (1.5 µm of underfocus) to a total dose of 5 DPA, showing that the helium bubble size and density increases with dose and irradiation temperature.

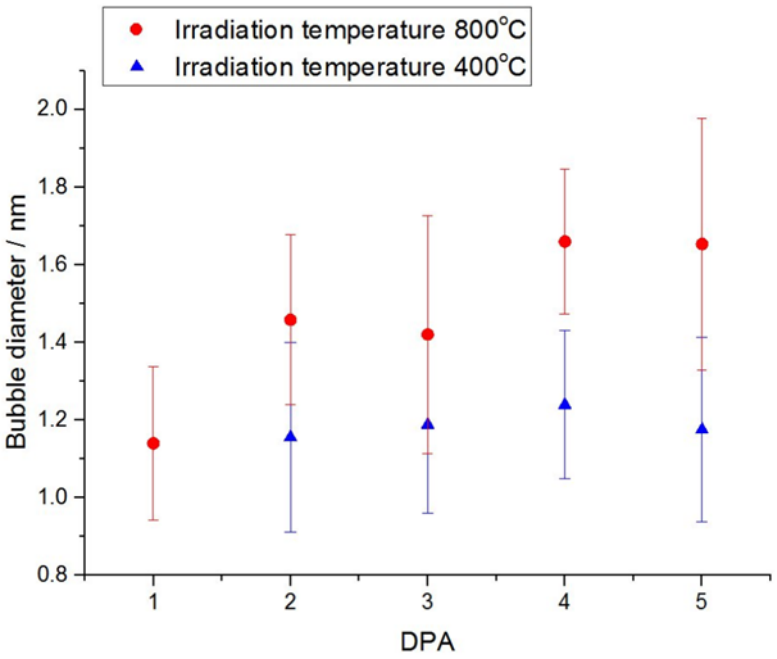

Figure 5. Plot of bubble diameter against DPA for SiC samples irradiated with 20 keV He ions at 400 and 800°C showing that bubble size increases with dose for both irradiations. However, He bubble nucleation occurs faster and bubble diameter increases more rapidly with the increased irradiation temperature of 800°C.

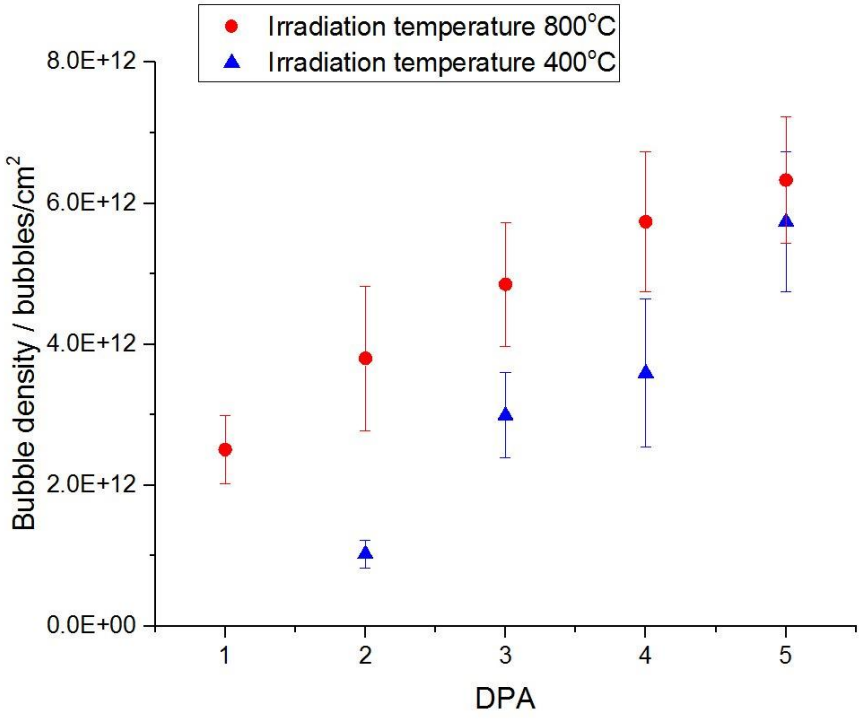

Figure 6. Plot of helium bubble areal density against DPA for SiC samples irradiated with 20 keV He ions at 400 and 800°C showing that bubble density increases with dose for both irradiations; however, helium bubble nucleation occurs faster and bubble diameter increases more rapidly at the increased irradiation temperature of 800°C.

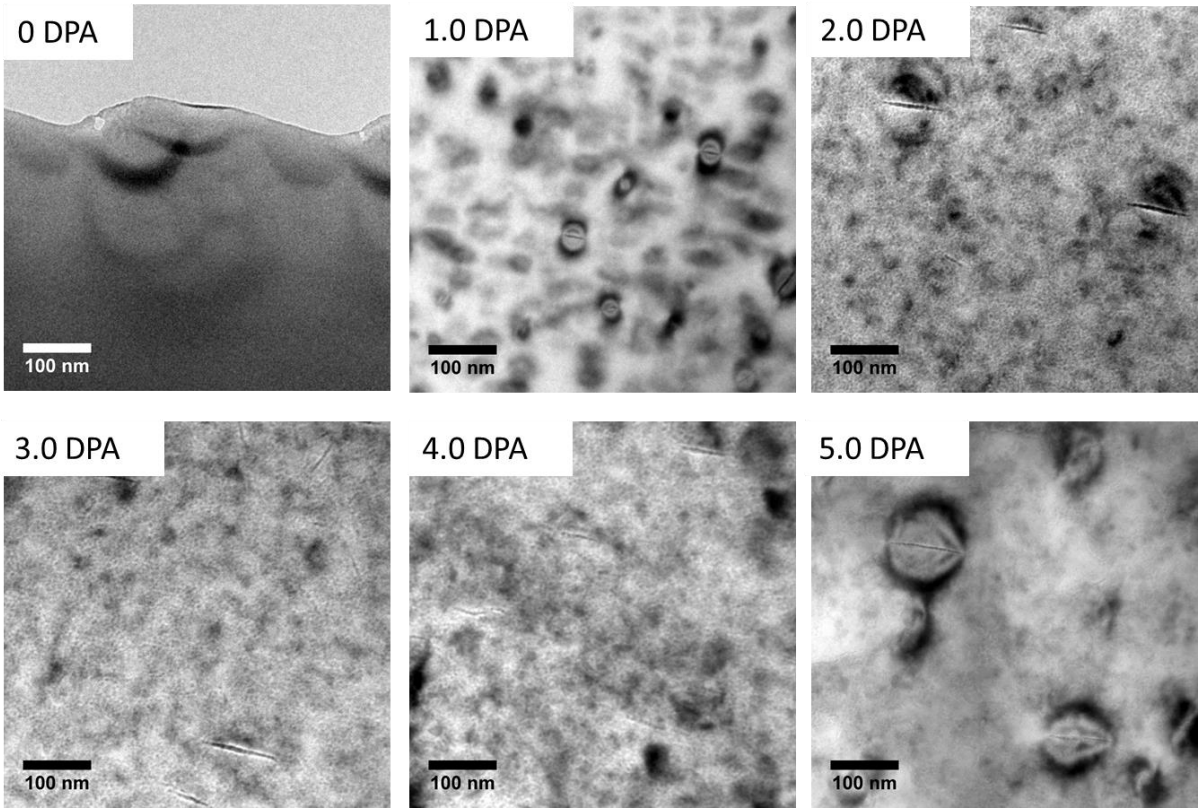

Figure 7. BF-TEM images captured of SiC irradiated with 20 keV He ions at 1200°C (1.5 µm of overfocus) labelled with damage dose received (DPA) showing the nucleation and growth of helium platelets and helium bubble discs.

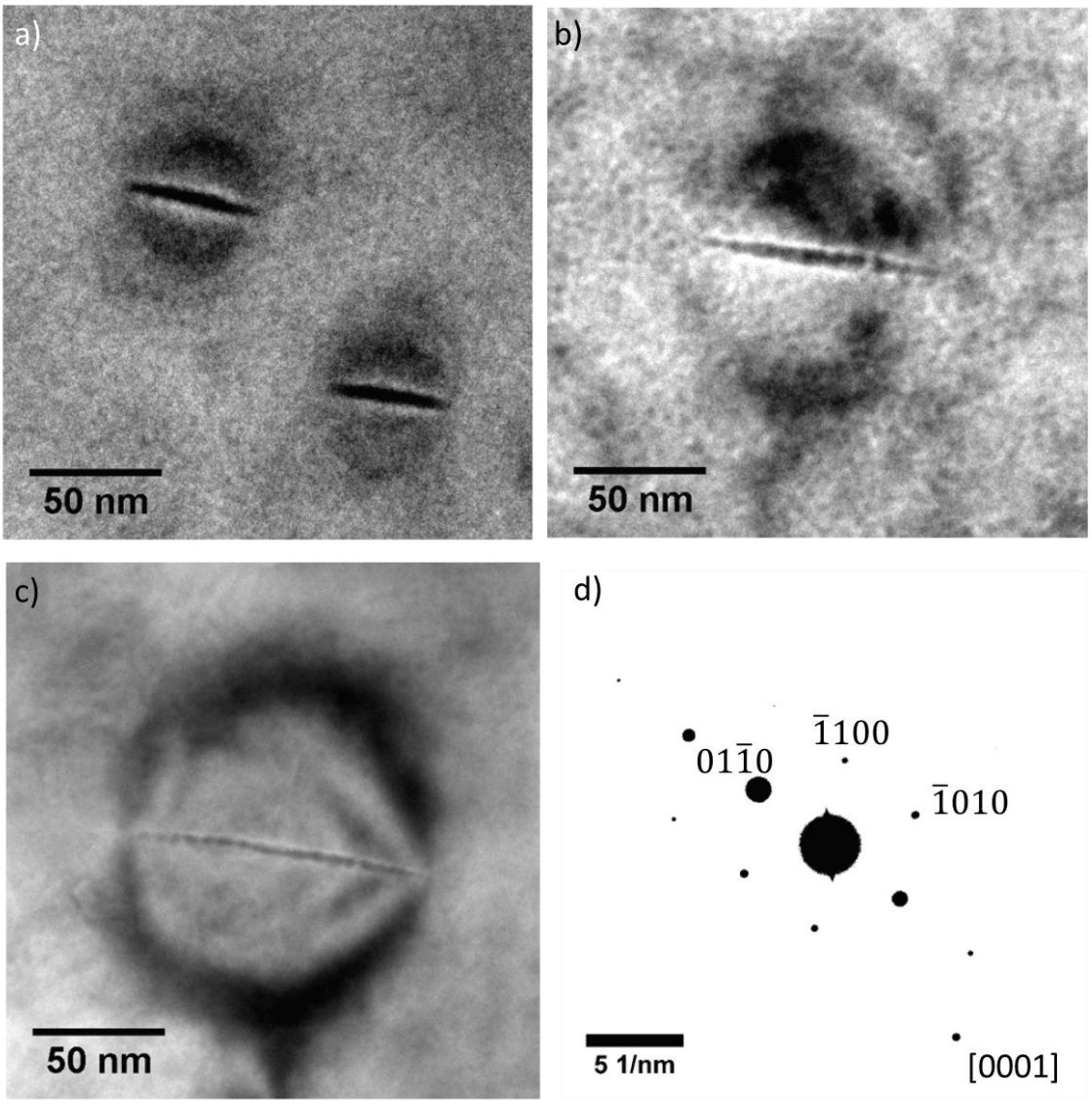

Figure 8. BF-TEM images of SiC sample irradiated with 20 keV He ions at 1200°C (1.5 µm of overfocus) orientated in the [0001] direction showing helium platelet evolution at a) 1.0, b) 2.0 and c) 5.0 DPA. It can be seen at low dose (1.0 DPA) that the platelet has no clear structure indicating a single helium filled cavity whereas at higher doses (2.0 and 5.0 DPA) individual cavities can be discerned d) SADP showing platelets orientation in a, b and c is along $\{\bar{\mathbf{1}}\mathbf{100}\}$ planes (corrected for rotation between micrograph and DP in TEM).

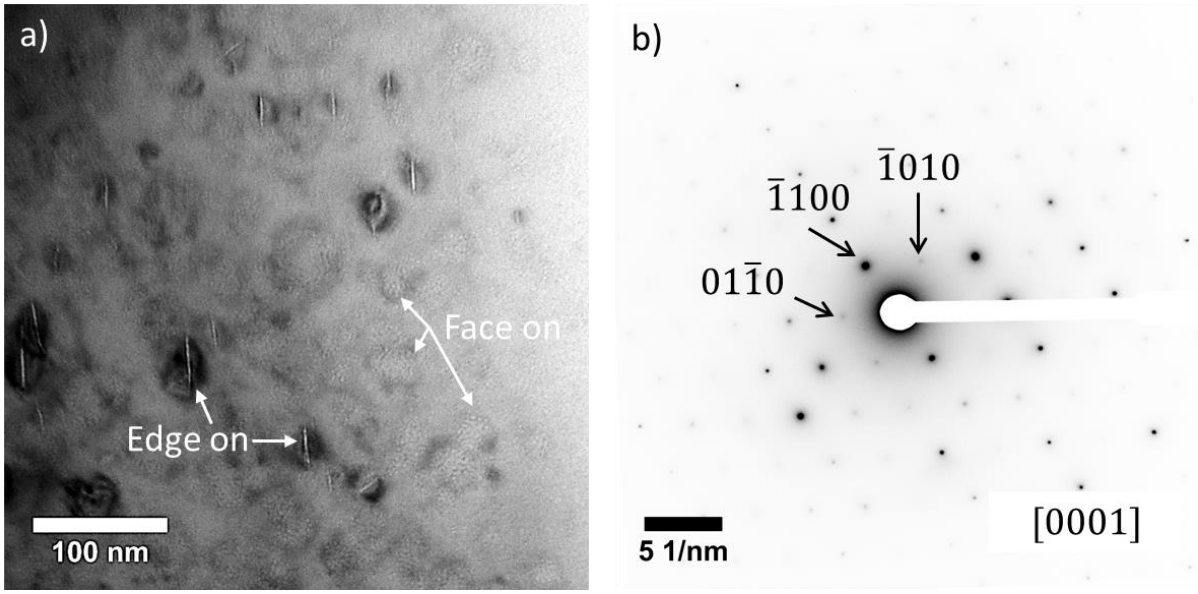

Figure 9. a) BF-TEM image of SiC sample irradiated with 20 keV He at 1200°C to 2.0 DPA (1.5 µm underfocus) showing helium platelets predominantly orientated face-on between the {0001} planes with some edge-on platelets aligned with the {$\mathbf{01\bar{1}0}$} planes and b) SADP of the region in a) (corrected for rotation between micrograph and DP in TEM).

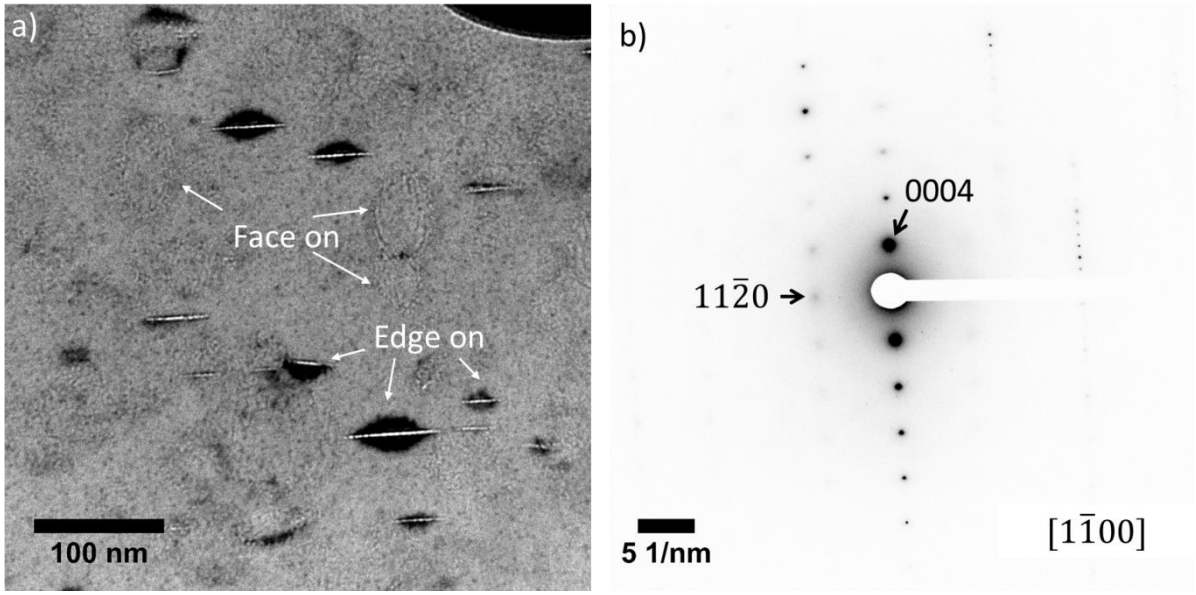

Figure 10 a) BF-TEM image of SiC irradiated with 20 keV He at 1200°C to 2.0 (1.5 µm underfocus) showing platelets predominantly orientated between {0001} planes but some face-on platelets and b) SADP of region in a) (corrected for rotation between micrograph and DP in TEM).

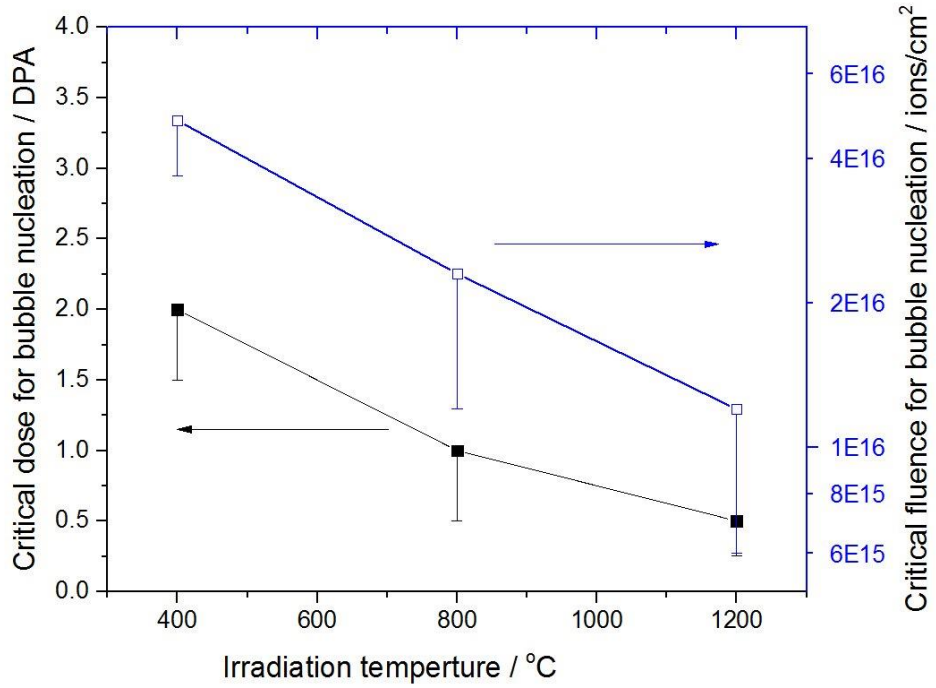

Figure 11. Plot of critical threshold for bubble nucleation in DPA and ions.cm^{-2} for SiC samples irradiated with 20 keV He ions to a He-appm/DPA ratio of ~2300 showing that the critical dose decreases with irradiation temperature (the error bars extending in the negative direction in the plots of critical DPA and dose are due to the electron beam being off during irradiation and so bubble nucleation may have occurred at any point during that irradiation step).